Journal of Materials Chemistry A

ROYAL SOCIETY OF CHEMISTRY

PAPER

View Article Online
View Journal | View Issue



Cite this: J. Mater. Chem. A, 2023, 11, 11748

# Enhancing the cycling stability of $MgH_2$ using nitrogen modified titanate†

Ren Zou,‡[ab] Jialing Li,‡[ab] Weijin Zhang,[a] Gangtie Lei,[b] Zhi Li[c] and Hujun Cao *[ad]

Received 15th March 2023
Accepted 3rd May 2023

DOI: 10.1039/d3ta01557b

rsc.li/materials-a

By introducing nitrogen anions, we obtained a N-doped $K_2Ti_6O_{13}$ (N-KTiO) catalyst with a considerably reduced band gap. The experimental results showed that N-KTiO could improve the de/re-hydrogenation kinetics and long-term cycling stability of the $Mg/MgH_2$ system. In particular, the peak temperature of $MgH_2$ with a 5 wt% N-KTiO catalyst was *ca.* 45 °C and 80 °C lower than those of $TiO_2$ catalysed and pure ones, respectively. After full dehydrogenation, 4.6 wt% $H_2$ was absorbed in 1 hour, even under room temperature. Moreover, after cycling for two hundred times at 300 °C, the $H_2$ capacity remained at 6.8 wt% with a retention as high as 94.4%, which is significantly better than those of the reported $MgH_2$-$TiO_2$ composites. Further investigation reveals that band structure changes of the catalyst may affect the catalytic effects, and the reversible changes in the valence state of the titanium species in catalysts are intrinsically associated with the enhanced kinetic properties and stability. This research may offer novel insights into developing effective catalysts for light metal hydrogen storage materials.



[a]Dalian Institute of Chemical Physics, Chinese Academy of Sciences, Dalian, 116023, China
[b]Key Laboratory of Environmentally Friendly Chemistry and Applications of Ministry of Education, School of Chemistry, Xiangtan University, Hunan, 411105, China
[c]National Engineering Research Center of Coal Gasification and Coal-Based Advanced Materials, Shandong Energy Group Co. LTD, Jinan, 250000, China
[d]Centre of Materials Science and Optoelectronics Engineering, University of Chinese Academy of Sciences, Beijing, 100049, China

† Electronic supplementary information (ESI) available. See DOI: https://doi.org/10.1039/d3ta01557b

‡ Zou Ren and Jialing Li contributed equally to this work.

*Hujun Cao is an Associate Professor at Dalian Institute of Chemical Physics (DICP), CAS, China. He started this position in 2018 after completing 4 years of postdoctoral research at Helmholtz-Zentrum Geesthacht (HZG, Dr Martin Dornheim's group), Germany. He obtained his PhD in chemical physics from DICP in 2014 under the supervision of Prof. Ping Chen and Prof. Jieshan Qiu. His research interests cover synthesis, characterization and utilization of metal hydride-based materials for hydrogen storage and ionic conductors. Recently, he has particularly focused on the development of novel hydride ion conductors.*

## 1. Introduction

Due to its high mass-energy density, adequate resources, variety of uses, and eco-friendliness, hydrogen has long been regarded as one of the most promising clean energy carriers.[1,2] However, the safe, efficient and economical transportation and storage of hydrogen have been a bottleneck for its practical applications.[3] To overcome this challenge, various hydrogen storage solutions were developed, such as solid-state materials,[4] physical adsorption materials,[5] liquid organic hydrogen carriers[6] and so on. The large hydrogen capacity of $MgH_2$ (theoretically up to 7.6 wt% and 110 kg $m^{-3}$), along with abundance, reversibility, and non-toxicity make it one of the most attractive choices for solid-state hydrogen storage.[7]

However, the slow kinetics ($E_a$ = 161 kJ $mol^{-1}$) and high reaction enthalpy ($\Delta H$ = 75 kJ per mol $H_2$) of $Mg/MgH_2$ have hindered its large-scale commercial application from being realized yet.[8,9] Significant scientific progress has been made in the last 50 years to improve the hydrogen storage properties of $Mg/MgH_2$; various methods have been used for achieving kinetic/thermodynamic optimization: nanoconfining,[10] alloying,[11] compositing,[12] outfield assistance,[13,14] and catalyst addition,[15] for achieving kinetic/thermodynamic optimization. Among these methods, transition metal-based catalysts have drawn much attention. Previous theoretical investigations suggested that the interaction between the H 1s electron and the unsaturated d electrons of transition metals could weaken the Mg-H bonds in $MgH_2$ and enhance its dehydrogenation capability.[16] Most of the catalyst addition is focused on Ti, V, Nb, Fe, Co, and Ni, as well as their compounds. Due to their good

catalytic dehydrogenation performance and cycling stability, Ti-based catalysts have attracted great interest.

Recently, titanium dioxide, especially *in situ* reduced and nano-sized titanium dioxide, has been widely studied for its ability to significantly improve the hydrogenation and dehydrogenation kinetics of magnesium hydride.[17,18] Our earlier research also showed that $TiO_2$ reduced by alkali metal hydrides is an efficient catalyst for improving the hydrogen storage properties of $Mg/MgH_2$.[19,20] In line with previous reports,[21–23] we also observed a change in the valence state of the titanium species during long-term cycling and believe that an intimate contact between $Mg/MgH_2$ and additives was crucial for modifying the $H_2$ storage properties. However, conventional characterisation techniques that have been used are insufficient to fully clarify the reasons for the observed improvement. Recently, Chen *et al.* reported an electron–hole pair mechanism of $Co/TiO_2$ in the improvement of hydrogen storage properties of $MgH_2$.[24] They claimed that $TiO_2$ has electron–hole pairs under thermal conditions, and these electron–hole pairs help $MgH_2$ dissociate and facilitate the process of dehydrogenation. Regrettably, the authors did not perform targeted characterization experiments to support their hypothesis. Anion doping is a common strategy to activate and change the band gap of $TiO_2$. Asahi *et al.* calculated the density of states (DOSs) of the substitutional doping of C, N, F, P, or S for O in the anatase $TiO_2$ crystal and showed that substitutional doping of N was the most effective because its p states contribute to narrowing the band-gap by mixing with O 2p states.[25]

Inspired by these previous studies on modified $TiO_2$,[26–28] we synthesized an N anion-doped $K_2Ti_6O_{13}$ catalyst by reducing $TiO_2$ with $KNH_2$, which exhibited a stable catalytic effect over 200 cycles with a retention rate of 94.4% (6.8 wt% $H_2$), and also provided a new perspective to understand the impact of band gap variations on the catalytic effects on $Mg/MgH_2$.

## 2. Results and discussion

### 2.1 Characterization of N-KTiO

Based on the early exploratory experiments (Fig. S1†), we prepared a potassium amide-reduced $TiO_2$ catalyst (named N-KTiO) by ball milling $KNH_2$ and $TiO_2$ at a mass ratio of 0.33 : 1 for 3 h and then annealing them at 450 °C for 5 h. The as-prepared N-KTiO catalyst was characterized by scanning electron microscopy (SEM), energy-dispersive X-ray spectroscopy (EDS), powder X-ray diffraction (XRD), X-ray photoelectron spectroscopy (XPS) and UV-Vis diffuse reflection spectroscopy (UV-Vis DRS) techniques. The phase characterization of pure $TiO_2$ and N-KTiO was studied as shown in Fig. S2.† It was observed that the diffraction peaks of $TiO_2$ were significantly weakened after ball-milling with $KNH_2$, suggesting that $TiO_2$ transformed into an amorphous phase (defect-rich $TiO_{2-x}$) which covers the surface of the catalyst during the mechanical ball milling process.[29] However, XRD is unable to determine the phase composition in the N-KTiO catalyst. FT-IR spectra of the precursor and N-KTiO are summarized in Fig. S3;† there are weak N–H stretching vibration peaks present in the precursor, while it is almost absent in N-KTiO. Indicating that after annealing, the decomposition of $KNH_2$ in N-KTiO was nearly completed. The thermal decomposition properties of the precursor were investigated using a homemade temperature-programmed desorption system equipped with a mass spectrometer (TPD-MS). The TPD-MS result shows that during the annealing procedure, the residual potassium amide in the precursor decomposes to ammonia and nitrogen (Fig. S4†).

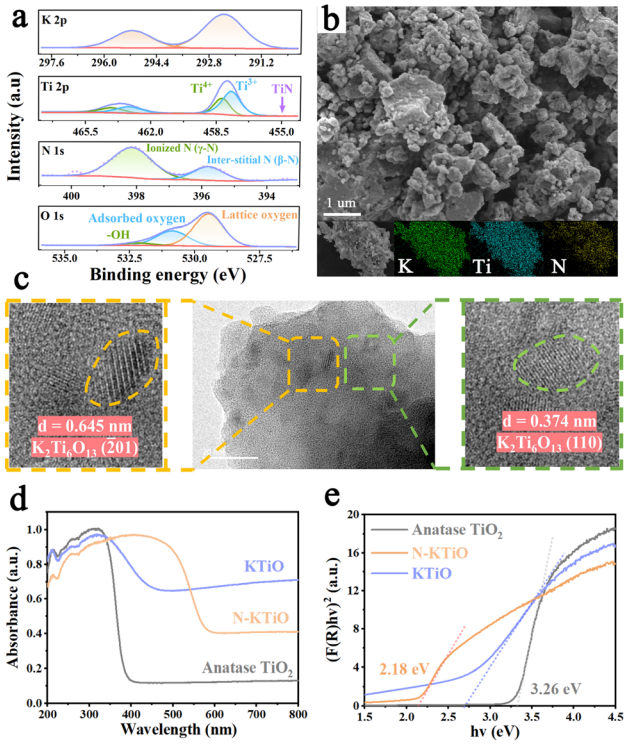


Fig. 1 (a) High-resolution XPS spectra of N-KTiO, including K 2p, Ti 2p, N 1s, and O 1s; (b) SEM micrograph and EDS mapping of N-KTiO; (c) HRTEM images of N-KTiO; (d) UV-Vis DRS of anatase $TiO_2$, the KTiO and N-KTiO samples; and their (e) Tauc plots (direct gaps, $n = 1/2$).

We collected the high-resolution X-ray photoelectron spectroscopy spectra of K 2p, Ti 2p, N 1s and O 1s to understand their chemical states (Fig. 1a). In the K 2p spectrum, two peaks located at 292.3 and 295.2 eV can be detected and ascribed to K $2p_{3/2}$ and K $2p_{1/2}$, respectively.[30] A peak belonging to $Ti^{3+}$ located at 457.8 eV is detected in the Ti 2p spectrum, which directly evidenced that titanium dioxide was partially reduced.[31] We noted that there is no peak corresponding to TiN at 455.0 eV, suggesting that no TiN was formed.[32] In the case of N 1s, the XPS spectrum shows a strong peak located at 398.2 eV with a neighbouring broad shoulder at 395.7 eV, implying that there are two chemical states for N. According to a previous report,[33] these peaks mainly originate from ionized N (γ-N) in the O–Ti–N ring and the interstitial N (β-N) in the lattice, respectively, indicating that N-KTiO exhibits N doping at both substitutional and interstitial sites and that some O sites in the titanate crystal were occupied by substitutional doping sites of N. The O 1s peak located at 529.5 eV involved lattice oxygen, while the peak at 531.2 eV resulted from the chemisorption of oxygen vacancies. This further showed that the oxygen vacancy was stabilized by

the adsorbed oxygen species, which is a characteristic of defect-rich oxides.[34]

We examined the morphology of N-KTiO by scanning electron microscopy as shown in Fig. 1b, which revealed that the N-KTiO particles are irregularly shaped and range from 0.1 to 1 μm in size. We used energy-dispersive X-ray spectroscopy mapping to reveal the uniform distribution of K, Ti and N species on the surface of N-KTiO. We further determined the structure of N-KTiO by high-resolution TEM as shown in Fig. 1c. We calculated the lattice spacings of 0.645 and 0.374 nm that were consistent with the (201) and (110) crystal planes of $K_2Ti_6O_{13}$, respectively. Lastly, we collected the collected UV-visible diffuse reflectance spectrum data as shown in Fig. 1d. The light absorption onset shifts from 380 nm for pure anatase $TiO_2$ to 580 nm for N-KTiO in the visible region. Notably, the KTiO samples (as-milled KH and $TiO_2$ at a mass ratio of 0.33 : 1 for 3 h) have shown an onset absorbance wavelength of 500 nm, showing that the substitutional doping of N has an important effect on the band gap. Based on these experimental results, we believe that the N anion-doped $K_2Ti_6O_{13}$ has been obtained,[35] leading to significant changes in the light absorption properties. An apparent decrease in the band gap of N-KTiO as compared with the pure anatase $TiO_2$ and KTiO was observed (Fig. 1e and S5†).

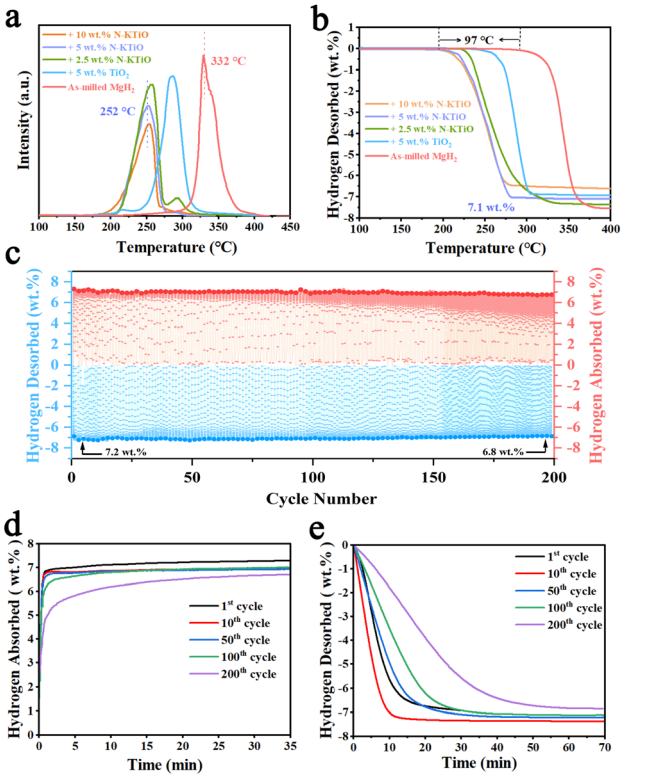


Fig. 2 (a) TPD-MS and (b) volumetric dehydrogenation curves of the as-milled $MgH_2$, $MgH_2$ catalysed with 5 wt% $TiO_2$ and the +$x$ wt% N-KTiO samples where $x = 2.5$, 5, and 10; (c) reversibility measurement of the +5 wt% N-KTiO sample at 300 °C under 0.3 and 30 bars of $H_2$ for de/re-hydrogenation; (d) hydrogenation and (e) dehydrogenation kinetics during different cycles.

## 2.2 Catalytic effect of N-KTiO

The optimum doping amount of catalyst on $MgH_2$ was investigated by ball-milling $MgH_2$ with $x$ wt% N-KTiO ($x = 0$, 2.5, 5, 10). Thermal decomposition properties of the N-KTiO doped $MgH_2$ were determined from hydrogen release curves obtained from TPD-MS as shown in Fig. 2a. The results showed that N-KTiO performs better than pure $TiO_2$. Considering the high $H_2$ content and similar peak temperatures of 5 and 10 wt% catalyst doping, we selected the +5 wt% N-KTiO sample for further investigations. Compared to the as-milled $MgH_2$ and pure $TiO_2$ catalysed $MgH_2$, its peak temperature was approximately *ca.* 80 and 45 °C lower, respectively. The volumetric dehydrogenation curves in Fig. 2b corresponded to the TPD-MS results. As expected, the N-KTiO catalyst could notably improve the hydrogen storage capacity of $MgH_2$.

Subsequently, we investigated the reversible hydrogen absorption properties of +5 wt% N-KTiO at room temperature under 1, 10, 30, and 50 bars of $H_2$ as shown in Fig. S6.† The composite had fast kinetics of $H_2$ absorption: it absorbed *ca.* 5.0 and 4.5 wt% $H_2$ within the first 1 h under 50 and 30 bars of $H_2$, respectively; moreover, it absorbed 4.2 wt% $H_2$ in 5 hours under 1 bar of $H_2$. In comparison, the as-milled $MgH_2$ absorbed less than 1 wt% of $H_2$ in 10 hours during re-hydrogenation. We also measured the isothermal dehydrogenation properties and the results are shown in Fig. S7.† We observed that +5 wt% N-KTiO had faster kinetics: it released *ca.* 4.2 wt% $H_2$ in 30 min at 260 °C and *ca.* 7.0 wt% $H_2$ in less than 10 min at 300 °C. Meanwhile, the as-milled $MgH_2$ barely released any $H_2$ even at 300 °C during the same period.

Fig. 2c shows the cycling stability and hydrogen storage capacity of the +5 wt% N-KTiO sample at 300 °C under 0.3 and 30 bars of $H_2$ backpressure for desorption (90 min) and absorption (60 min), respectively. The reversible hydrogen capacity decayed from *ca.* 7.2 to 6.8 wt% after two hundred cycles. The retention was as high as 94.4%, which could well meet the requirements of long-term use of on-board hydrogen storage devices. As a comparison, after 20 cycles, the retention amount of unmodified commercial magnesium hydride was less than 80%.[36] Fig. 2d and e show the drop in kinetics during the cycling process which we attributed to the agglomeration of $Mg/MgH_2$ and precipitation of the catalyst from the bulk phase to the boundaries with $Mg/MgH_2$, as we will be discussed later.

## 2.3 Kinetic and thermodynamic properties

We evaluated the dehydrogenation kinetics of +5 wt% N-KTiO by applying the Kissinger model to calculate the apparent activation energy ($E_a$). TPD-MS data of the as-milled $MgH_2$ and the +5 wt% N-KTiO were collected at heating rates of 2, 4, 6, and 8 °C $min^{-1}$ (Fig. 3a and b). We then fitted the obtained peak temperatures using the Kissinger plot (Fig. 3c and d). The slopes reveal that the +5 wt% N-KTiO sample has an apparent activation energy of 53 (±1.9) kJ $mol^{-1}$, which was *ca.* 55 kJ $mol^{-1}$ lower than that of the as-milled $MgH_2$. Compared with the $E_a$ of pristine $MgH_2$ (*ca.* 180 kJ $mol^{-1}$),[37] our results show that ball milling significantly reduces the activation energy of

 

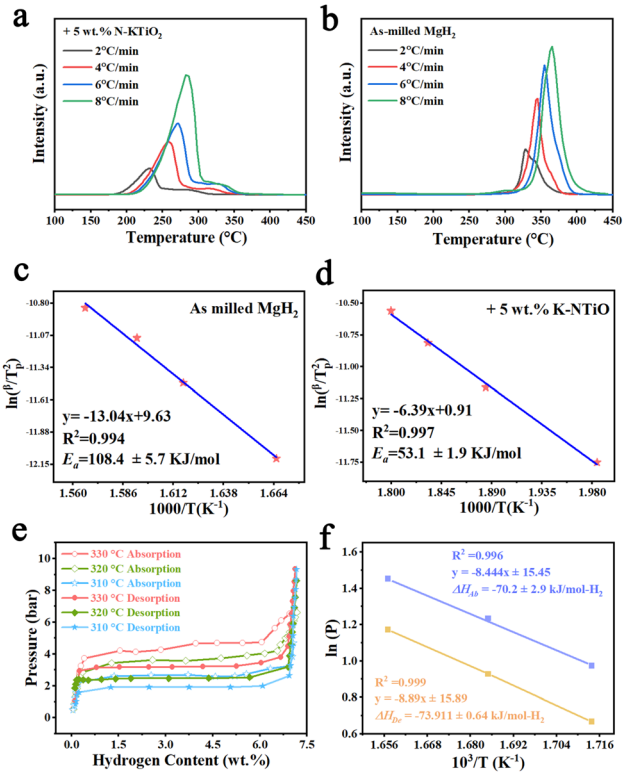


Fig. 3 TPD–MS curves of (a) the +5 wt% N-KTiO sample and (b) the as-milled $MgH_2$ at heating rates of 2, 4, 6, and 8 °C $min^{-1}$; Kissinger plot of (c) the +5 wt% N-KTiO sample and (d) the as-milled $MgH_2$; (e) PCI de/ab-sorption curves at 310, 320, and 330 °C, and (f) Van't Hoff plot of the +5 wt% N-KTiO sample.

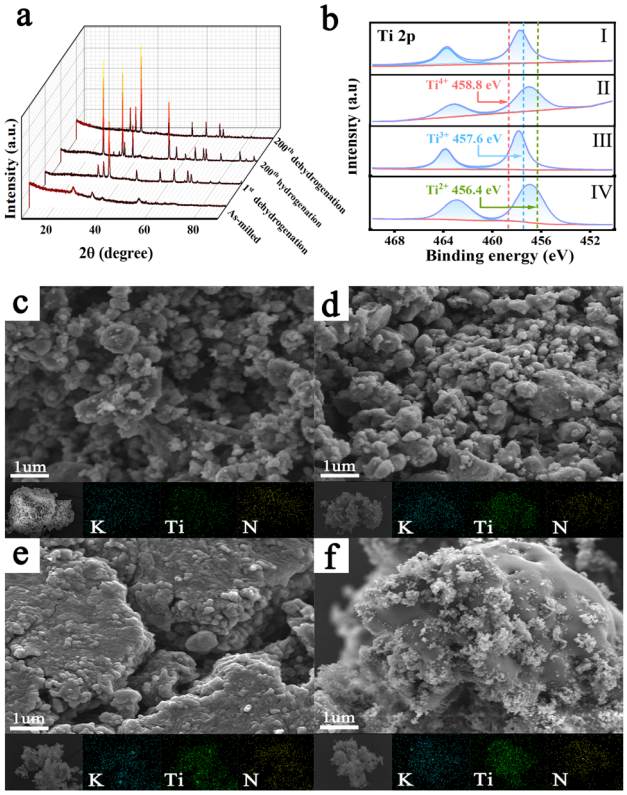


Fig. 4 (a) XRD patterns of the as-milled, dehydrogenated and hydrogenated (1st and 200th) samples; (b) Ti 2p XPS spectra of (I) the as-milled, (II) the 1st dehydrogenated, (III) the 200th hydrogenated, and (IV) the 200th dehydrogenated samples. SEM images and EDS mapping of (c) the as-milled, (d) the 1st dehydrogenated, (e) the 200th hydrogenated, and (f) the 200th dehydrogenated samples.

magnesium hydride, while the addition of a catalyst leads to further optimisation.

Another important parameter for hydrogen storage materials is the reaction enthalpy ($\Delta H$). We can easily derive such information from the PCI (pressure–composition–isotherm) curves using the Van't Hoff plot.[38] Fig. 3e shows a distinct plateau region at each isothermal curve for the PCI desorption and absorption measurements of the +5 wt% N-KTiO sample at 310, 320, and 330 °C. Meanwhile, Fig. 3f shows the Van't Hoff curve of equilibrium pressure *vs.* temperature. The reaction enthalpies of de/re-hydrogenation were determined to be *ca.* 70 (±2.9) kJ per mol $H_2$ and 74 (±0.64) kJ per mol $H_2$, which are slightly lower than those of the pristine magnesium hydride.[39] We believe that this might be related to the notable decrease in grain sizes caused by high-energy ball milling.[40]

### 2.4 Phase transition of N-KTiO during cycling

As revealed in Sections 2.2 and 2.3, the +5 wt% N-KTiO sample exhibits excellent de/re-hydrogenation cycling stability and improved de/re-hydrogenation kinetics. To better understand the interaction between the N-KTiO catalyst and $MgH_2$/Mg, it is necessary to further explore the phase transition on the N-KTiO doped sample during cycling. Fig. 4a displays the XRD patterns of the as-milled, dehydrogenated and hydrogenated (1st and 200th) samples. Although XRD patterns did not reflect any clear diffraction peaks of N-KTiO, peaks corresponding to Mg/$MgH_2$ are revealed clearly after dehydrogenation and hydrogenation. The full width at half maximum of the diffraction peaks (FWHM) belonging to the as-milled +5 wt% N-KTiO sample is relatively broad, which indicates that the grain size of $MgH_2$ decreases significantly during the ball milling process. However, the FWHM belonging to the post-cycling samples was much narrower, demonstrating that significant grain growth had occurred throughout the cycling process. Additionally, Fig. 4c and d display SEM micrographs of the as-milled and dehydrogenated (1st and 200th) composites. After cycling, we observed a notable increase in particle sizes. In particular, the EDS mapping of the samples shows an obvious aggregation of K and Ti species on the surface of $MgH_2$/Mg, suggesting that the increase of particle sizes is accompanied by the catalyst precipitation from the bulk phase.

To further clarify the chemical state transformations of Ti in the +5 wt% N-KTiO sample during cycling, we collected Ti 2p XPS spectra of the as-milled, dehydrogenated and hydrogenated (1st and 200th) samples as shown in Fig. 4b. Interestingly, the valence of the titanium species in the as-milled +5 wt% N-KTiO sample does not vary considerably compared to N-KTiO, but the peaks corresponding to Ti $2p_{1/2}$ and Ti $2p_{3/2}$ in the

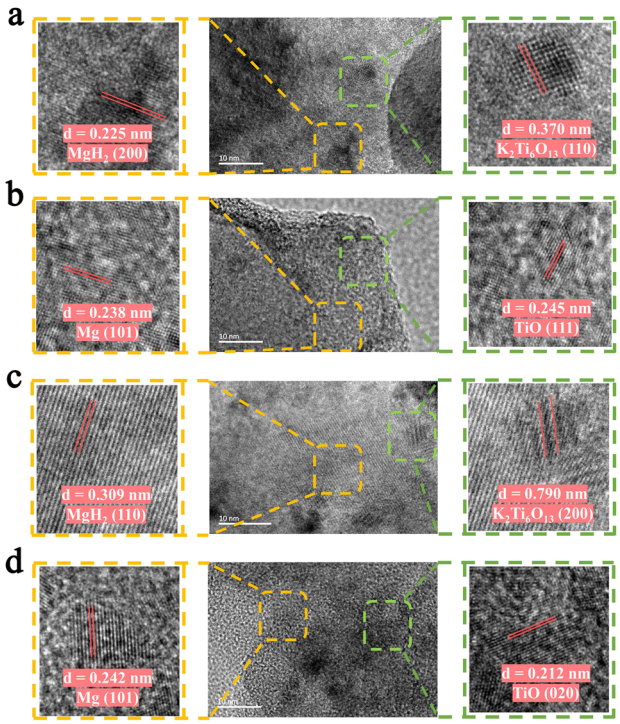


Fig. 5 HRTEM images of (a) the as-milled, (b) the 1st dehydrogenated, (c) the 200th hydrogenated, and (d) the 200th dehydrogenated samples.

dehydrogenated sample shifted towards lower binding energy, indicating the generation of low-valent titanium. This trend persists in subsequent cycles, indicating that this change in the valence of titanium caused by de/re-hydrogenation is reversible.

Fig. S8† displays TEM micrographs of the as-milled, dehydrogenated and hydrogenated (1st and 200th) samples. Clear precipitation of the catalytic phase onto the Mg surface is observed (Fig. S8d†). Moreover, with the aid of HRTEM, the phase transition of N-KTiO in the titanium species corresponding to the change of titanium valency was investigated. Fig. 5a shows HRTEM images of the as-milled sample; in addition to the lattice fringes of $MgH_2$, $K_2Ti_6O_{13}$ fringes at (110) planes are observed. After dehydrogenation (Fig. 5b), there are lattice fringes of TiO. Even after 200 cycles, the lattice fringes of $K_2Ti_6O_{13}$ and TiO are still present in the hydrogenated and dehydrogenated samples, which suggests that a reversible redox reaction with $H_2$ insertion and removal from the catalyst surface may have occurred during the cycling, similar to previous reports.[20,41,42]

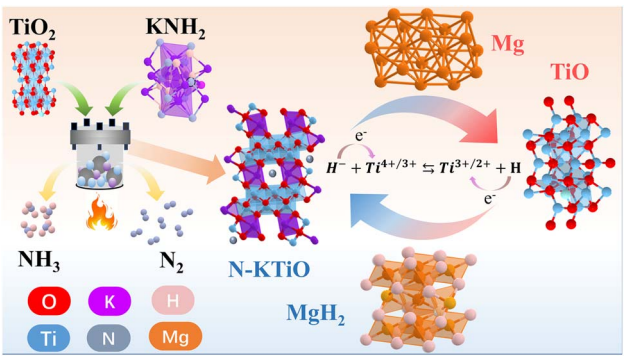


Fig. 6 Schematic diagram of the catalytic mechanism in de/re-hydrogenation of N-KTiO.

### 2.5 Possible catalytic mechanism of N-KTiO

Based on the above-mentioned experimental results and discussion, we propose a potential mechanism for the N-KTiO enhanced de/re-hydrogenation kinetics and cycling stability of $MgH_2$ in Fig. 6. First, the ball milling procedure creates stress that crushes the catalyst and enables it to come into contact with the $MgH_2$ boundary more closely and evenly. Additionally, the absorption/desorption kinetics of $Mg/MgH_2$ have improved considerably because of a significant reduction in the grain size of magnesium hydride.[43]

Second, the heating treatment introduces N anions into $K_2Ti_6O_{13}$. As shown by UV-Vis DRS results, N anion doping significantly reduces the band gap of N-KTiO (from 3.26 eV to 2.18 eV) and weakens the strength of the valence bond of N-KTiO compared to pure $TiO_2$. Therefore, it is easier for valence electrons to be excited to free electrons, resulting in a higher hole concentration.[44,45] This enables Ti ions to act as a better bridge for electron transfer between Mg and H ions,[46] because the Ti ions can gain electrons ($e^-$) more easily than Mg ions and lose $e^-$ more easily than $H^-$ ions.[21] Moreover, XPS and TEM results confirm that the valence state of titanium species changes reversibly during cycling. This reversible behaviour of the catalyst is believed to facilitate the re/de-hydrogenation processes of $Mg/MgH_2$. Since Ti's electronegativity (1.54) is between Mg's (1.31) and H's (2.2), multivalent titanium species may possibly weaken the Mg–H bond and promote hydrogen dissociation, which would result in $MgH_2$ exhibiting lower activation energy and faster dehydrogenation kinetics.[47]

Although some of the catalyst is precipitated from the $Mg/MgH_2$ bulk phase to the surface after cycles, as shown by SEM/TEM images of the +5 wt% N-KTiO sample at the 200th de/re-hydrogenation cycle. EDS mapping and HRTEM reveal that there are still many phase interfaces between the catalyst and $Mg/MgH_2$. These interfaces may inhibit particle growth and agglomeration. Moreover, multivalent titanium species at interfaces may act as diffusion channels for electron and hydrogen transfer during absorption and desorption, which may contribute to the long-term cycling stability and enhanced $H_2$ storage properties of the N-KTiO doped sample.

## 3. Conclusions

In summary, we synthesized N-KTiO by introducing nitrogen anions and demonstrated its excellent catalytic effects on $Mg/MgH_2$. The +5 wt% N-KTiO sample showed low onset and peak dehydrogenation temperatures of 195 and 252 °C, respectively. It also absorbed *ca.* 5.0 wt% $H_2$ within the first hour at room temperature under 50 bar $H_2$. Moreover, it maintained its improved hydrogen storage performance for at least 200 cycles

 

with a retention of 94.4% (6.8 wt% $H_2$). The introduction of N-KTiO into $MgH_2$ resulted in a halved activation energy for dehydrogenation compared to pristine $MgH_2$, while the enthalpy has not changed significantly, implying that N-KTiO mainly acted as a catalyst. Further investigation revealed that a redox reaction on the catalyst surface occurred during the de/re-hydrogenation cycle, leading to a reversible change in the valence of titanium. Multivalent titanium species at the interfaces between the catalyst and $Mg/MgH_2$ may act as diffusion channels for electrons and hydrogen during absorption and desorption. In this direction, additional research is required to determine the *in situ* phase composition variation of the catalyst-to-$Mg/MgH_2$ interfaces and to understand how N doping affects the bonding strength between Mg and hydrogen. Our ongoing research focuses on these areas.

## Conflicts of interest

There are no conflicts to declare.

## Acknowledgements

The authors acknowledge the project supported by the National Key Research and Development Program of China (2021YFB4000602), the Key Research and Development Program of Shandong Province, China (2020CXGC010402), the National Natural Science Foundation of China (22279130), and the Youth Innovation Promotion Association CAS (2019189). The authors also would like to acknowledge Prof. Ping Chen for stimulating the discussions.

## Notes and references

1 T. He, H. J. Cao and P. Chen, *Adv. Mater.*, 2019, **31**, 1902757.
2 F. Wang, J. D. Harindintwali, Z. Yuan, M. Wang, F. Wang, S. Li, Z. Yin, L. Huang, Y. Fu, L. Li, S. X. Chang, L. Zhang, J. Rinklebe, Z. Yuan, Q. Zhu, L. Xiang, D. C. W. Tsang, L. Xu, X. Jiang, J. Liu, N. Wei, M. Kästner, Y. Zou, Y. S. Ok, J. Shen, D. Peng, W. Zhang, D. Barceló, Y. Zhou, Z. Bai, B. Li, B. Zhang, K. Wei, H. Cao, Z. Tan, L.-b. Zhao, X. He, J. Zheng, N. Bolan, X. Liu, C. Huang, S. Dietmann, M. Luo, N. Sun, J. Gong, Y. Gong, F. Brahushi, T. Zhang, C. Xiao, X. Li, W. Chen, N. Jiao, J. Lehmann, Y.-G. Zhu, H. Jin, A. Schäffer, J. M. Tiedje and J. M. Chen, *The Innovation*, 2021, **2**, 100180.
3 L. Schlapbach and A. Züttel, *Mater. Sustainable Energy*, 2001, **414**, 265–270.
4 P. Chen, Z. Xiong, J. Luo, J. Lin and K. L. Tan, *Nature*, 2002, **420**, 302–304.
5 K. K. Gangu, S. Maddila, S. B. Mukkamala and S. B. Jonnalagadda, *J. Energy Chem.*, 2019, **30**, 132–144.
6 Z. Jing, Q. Yuan, Y. Yu, X. Kong, K. C. Tan, J. Wang, Q. Pei, X.-B. Wang, W. Zhou, H. Wu, A. Wu, T. He and P. Chen, *ACS Mater. Lett.*, 2021, **3**, 1417–1425.
7 Y. Shang, C. Pistidda, G. Gizer, T. Klassen and M. Dornheim, *J. Magnesium Alloys*, 2021, **9**, 1837–1860.
8 J. Zhang, Y. Zhu, L. Yao, C. Xu, Y. Liu and L. Li, *J. Alloys Compd.*, 2019, **782**, 796–823.
9 Q. Luo, J. Li, B. Li, B. Liu, H. Shao and Q. Li, *J. Magnesium Alloys*, 2019, **7**, 58–71.
10 Y. Jia and X. Yao, *Int. J. Hydrogen Energy*, 2017, **42**, 22933–22941.
11 M. Zhu, H. Wang, L. Z. Ouyang and M. Q. Zeng, *Int. J. Hydrogen Energy*, 2006, **31**, 251–257.
12 W. Lin, X. Xiao, X. Wang, J.-W. Wong, Z. Yao, M. Chen, J. Zheng, Z. Hu and L. Chen, *J. Energy Chem.*, 2020, **50**, 296–306.
13 X. Zhang, Y. Sun, S. Ju, J. Ye, X. Hu, W. Chen, L. Yao, G. Xia, F. Fang, D. Sun and X. Yu, *Adv. Mater.*, 2023, **35**, e2206946.
14 R. Zou, J. A. Bolarin, G. T. Lei, W. B. Gao, Z. Li, H. J. Cao and P. Chen, *Chem. Eng. J.*, 2022, **450**, 138072.
15 R. A. Varin, L. Zbroniec, M. Polanski and J. Bystrzycki, *Energies*, 2011, **4**, 1–25.
16 B. Liu, B. Zhang, Y. Wu, W. Lv and S. Zhou, *Int. J. Hydrogen Energy*, 2019, **44**, 27885–27895.
17 L. Ren, W. Zhu, Y. Li, X. Lin, H. Xu, F. Sun, C. Lu and J. Zou, *Nano-Micro Lett.*, 2022, **14**, 144.
18 J. Zhang, R. Shi, Y. Zhu, Y. Liu, Y. Zhang, S. Li and L. Li, *ACS Appl. Mater. Interfaces*, 2018, **10**, 24975–24980.
19 M. Dai, J. A. Bolarin, G. Lei, Z. Li, T. He, H. Cao and P. Chen, *J. Alloys Compd.*, 2022, **897**, 162750.
20 J. A. Bolarin, Z. Zhang, H. Cao, Z. Li, T. He and P. Chen, *J. Magnesium Alloys*, 2021, DOI: **10.1016/j.jma.2021.11.005**.
21 J. Cui, H. Wang, J. Liu, L. Ouyang, Q. Zhang, D. Sun, X. Yao and M. Zhu, *J. Mater. Chem. A*, 2013, **1**, 5603–5611.
22 Q. Kong, H. Zhang, Z. Yuan, J. Liu, L. Li, Y. Fan, G. Fan and B. Liu, *ACS Sustainable Chem. Eng.*, 2020, **8**, 4755–4763.
23 D. Pukazhselvan, N. Nasani, P. Correia, E. Carbó-Argibay, G. Otero-Irurueta, D. G. Stroppa and D. P. Fagg, *J. Power Sources*, 2017, **362**, 174–183.
24 M. Chen, X. Z. Xiao, M. Zhang, J. G. Zheng, M. J. Liu, X. C. Wang, L. J. Jiang and L. X. Chen, *Int. J. Hydrogen Energy*, 2019, **44**, 15100–15109.
25 R. Asahi, T. Morikawa, T. Ohwaki, K. Aoki and Y. Taga, *Science*, 2001, **293**, 269–271.
26 A. Naldoni, M. Altomare, G. Zoppellaro, N. Liu, S. Kment, R. Zboril and P. Schmuki, *ACS Catal.*, 2019, **9**, 345–364.
27 X. Chen, L. Liu, P. Y. Yu and S. S. Mao, *Science*, 2011, **331**, 746–750.
28 T. S. Rajaraman, S. P. Parikh and V. G. Gandhi, *Chem. Eng. J.*, 2020, **389**, 123918.
29 V. A. Zuñiga-Ibarra, S. Shaji, B. Krishnan, J. Johny, S. Sharma Kanakkillam, D. A. Avellaneda, J. A. A. Martinez, T. K. D. Roy and N. A. Ramos-Delgado, *Appl. Surf. Sci.*, 2019, **483**, 156–164.
30 D. Courcot, L. Gengembre, M. Guelton, Y. Barbaux and B. Grzybowska, *J. Chem. Soc., Faraday Trans.*, 1994, **90**, 895–898.
31 F. Werfel and O. Brümmer, *Phys. Scr.*, 1983, **28**, 92.
32 D. Jaeger and J. Patscheider, *J. Electron Spectrosc. Relat. Phenom.*, 2012, **185**, 523–534.
33 M. Sathish, B. Viswanathan, R. P. Viswanath and C. S. Gopinath, *Chem. Mater.*, 2005, **17**, 6349–6353.

34 K. Ye, K. Li, Y. Lu, Z. Guo, N. Ni, H. Liu, Y. Huang, H. Ji and P. Wang, *TrAC, Trends Anal. Chem.*, 2019, **116**, 102–108.
35 H. Akihiko, Y. Miwako, T. Hiroaki and I. Seishiro, *Chem. Lett.*, 1998, **27**, 707–708.
36 L. Zhang, F. M. Nyahuma, H. Zhang, C. Cheng, J. Zheng, F. Wu and L. Chen, *Green Energy Environ.*, 2023, **8**, 589–600.
37 I. E. Malka, T. Czujko and J. Bystrzycki, *Int. J. Hydrogen Energy*, 2010, **35**, 1706–1712.
38 J. F. Stampfer Jr, C. E. Holley Jr and J. F. Suttle, *J. Am. Chem. Soc.*, 1960, **82**, 3504–3508.
39 A. S. Pedersen, J. Kjøller, B. Larsen and B. Vigeholm, *Int. J. Hydrogen Energy*, 1983, **8**, 205–211.
40 M. Paskevicius, D. A. Sheppard and C. E. Buckley, *J. Am. Chem. Soc.*, 2010, **132**, 5077–5083.
41 S. Kumar, A. Mukherjee, S. Sonak and N. Krishnamurthy, *J. Nucl. Mater.*, 2013, **443**, 207–211.
42 T. Zhang, S. Isobe, A. Jain, Y. Wang, S. Yamaguchi, H. Miyaoka, T. Ichikawa, Y. Kojima and N. Hashimoto, *J. Alloys Compd.*, 2017, **711**, 400–405.
43 A. Zaluska, L. Zaluski and J. O. Ström–Olsen, *J. Alloys Compd.*, 1999, **288**, 217–225.
44 O. Carp, C. L. Huisman and A. Reller, *Prog. Solid State Chem.*, 2004, **32**, 33–177.
45 S. G. Kumar and L. G. Devi, *J. Phys. Chem. A*, 2011, **115**, 13211–13241.
46 G. Liu, L. Wang, Y. Hu, C. Sun, H. Leng, Q. Li and C. Wu, *J. Alloys Compd.*, 2021, **881**, 160644.
47 M. Zhang, X. Xiao, B. Luo, M. Liu, M. Chen and L. Chen, *J. Energy Chem.*, 2020, **46**, 191–198.